



HAL
open science

Infrared Photodetection Based on Colloidal Quantum-Dot Films with High Mobility and Optical Absorption up to THz

Emmanuel Lhuillier, Marion Scarafagio, Patrick Hease, Brice Nadal, Hervé Aubin, Xiang Zhen Xu, Nicolas Lequeux, Gilles Patriarche, Sandrine Ithurria, Benoit Dubertret

► **To cite this version:**

Emmanuel Lhuillier, Marion Scarafagio, Patrick Hease, Brice Nadal, Hervé Aubin, et al.. Infrared Photodetection Based on Colloidal Quantum-Dot Films with High Mobility and Optical Absorption up to THz. *Nano Letters*, 2016, 16 (2), pp.1282-1286. 10.1021/acs.nanolett.5b04616 . hal-01418828

HAL Id: hal-01418828

<https://hal.science/hal-01418828>

Submitted on 17 Dec 2016

HAL is a multi-disciplinary open access archive for the deposit and dissemination of scientific research documents, whether they are published or not. The documents may come from teaching and research institutions in France or abroad, or from public or private research centers.

L'archive ouverte pluridisciplinaire **HAL**, est destinée au dépôt et à la diffusion de documents scientifiques de niveau recherche, publiés ou non, émanant des établissements d'enseignement et de recherche français ou étrangers, des laboratoires publics ou privés.

Infrared Photodetection Based on Colloidal Quantum-Dot Films with High Mobility and Optical Absorption up to THz

Emmanuel Lhuillier,^{*,†,‡} Marion Scarafagio,^{†,§} Patrick Hease,[§] Brice Nadal,[†] Hervé Aubin,[§] Xiang Zhen Xu,[§] Nicolas Lequeux,[§] Gilles Patriarche,^{||} Sandrine Ithurria,[§] and Benoit Dubertret^{*,§}

[†]Nexdot, 10 rue Vauquelin, 75005 Paris, France

[‡]Institut des NanoSciences de Paris, UPMC-UMR CNRS 7588, 4 place Jussieu, 75252 Paris CEDEX 05, France

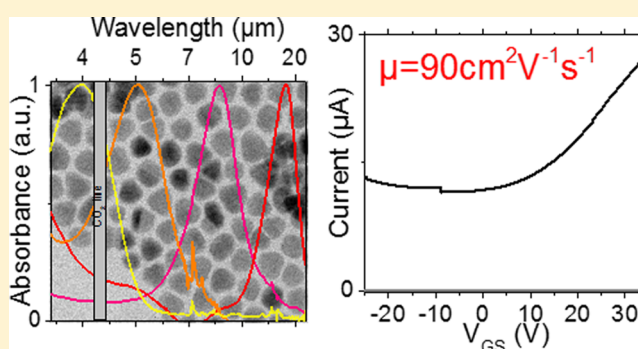
[§]Laboratoire de Physique et d'Etude des Matériaux, ESPCI-ParisTech, PSL Research University, Sorbonne Université UPMC Univ Paris 06, CNRS, 10 rue Vauquelin 75005 Paris, France

^{||}Laboratoire de Photonique et de Nanostructures, LPN/UPR20-CNRS, Route de Nozay, 91460 Marcoussis, France

Supporting Information

ABSTRACT: Infrared thermal imaging devices rely on narrow band gap semiconductors grown by physical methods such as molecular beam epitaxy and chemical vapor deposition. These technologies are expensive, and infrared detectors remain limited to defense and scientific applications. Colloidal quantum dots (QDs) offer a low cost alternative to infrared detector by combining inexpensive synthesis and an ease of processing, but their performances are so far limited, in terms of both wavelength and sensitivity. Herein we propose a new generation of colloidal QD-based photodetectors, which demonstrate detectivity improved by 2 orders of magnitude, and optical absorption that can be continuously tuned between 3 and 20 μm . These photodetectors are based on the novel synthesis of n-doped HgSe colloidal QDs whose size can be tuned continuously between 5 and 40 nm, and on their assembly into solid nanocrystal films with mobilities that can reach up to $100 \text{ cm}^2 \text{ V}^{-1} \text{ s}^{-1}$. These devices can be operated at room temperature with the same level of performance as the previous generation of devices when operated at liquid nitrogen temperature. HgSe QDs can be synthesized in large scale (>10 g per batch), and we show that HgSe films can be processed to form a large scale array of pixels. Taken together, these results pave the way for the development of the next generation mid- and far-infrared low-cost detectors and camera.

KEYWORDS: HgSe, colloidal quantum dot, transistor, electrolyte gating, photoresponse, mid- and far-infrared



Colloidal quantum dots (CQD) are excellent building blocks to develop low cost optoelectronic devices.¹ For applications in the visible wavelength range, CQD face competition with existing technologies such as CMOS, which already achieve high performance at low cost. In the infrared (IR), high performances detectors also exist based on technologies such as multiquantum well, InSb, HgCdTe, and type II superlattices. Their detectivities range from 5×10^{10} jones in the LWIR (8–12 μm) to 5×10^{11} jones in the MWIR (3–5 μm), while their noise equivalent temperature difference can be as low as 10 mK. However, they remain expensive and technologically demanding. Uncooled detectors such as the bolometer offer an interesting alternative to the cooled quantum detectors, but their performances remain lower ($D^* \approx \text{few } 10^9 \text{ jones}$). To overcome these limitations, new technologies that deliver fast,² high-performing uncooled³ detectors must be developed. Possible strategies rely on the use of plasmon for light concentration or hot electron collection.⁴ Material-like graphene are of utmost interest to

design new generation of bolometer,⁵ however, its low absorption limits its practical use. CQD films achieve absorption coefficients almost as large as the bulk values. As a result they may become a low-cost infrared alternative to current technologies as long as they can address the mid- and far-IR.

The performance of the CQD-based devices also crucially depends on their transport properties. The hopping effective mobility tends to be low ($\mu < 1 \text{ cm}^2 \text{ V}^{-1} \text{ s}^{-1}$). This has led to the development of alternative device geometries such as nanotrench⁶ or hybrid structures with graphene.⁷ Extensive efforts have been made to obtain nanocrystal solid with larger mobility. The latter is obtained using optimized surface passivation relying on atomically short^{8–10} or inorganic ligands.¹¹ Recent progress has pushed the carrier mobility¹²

Received: November 12, 2015

Revised: January 5, 2016

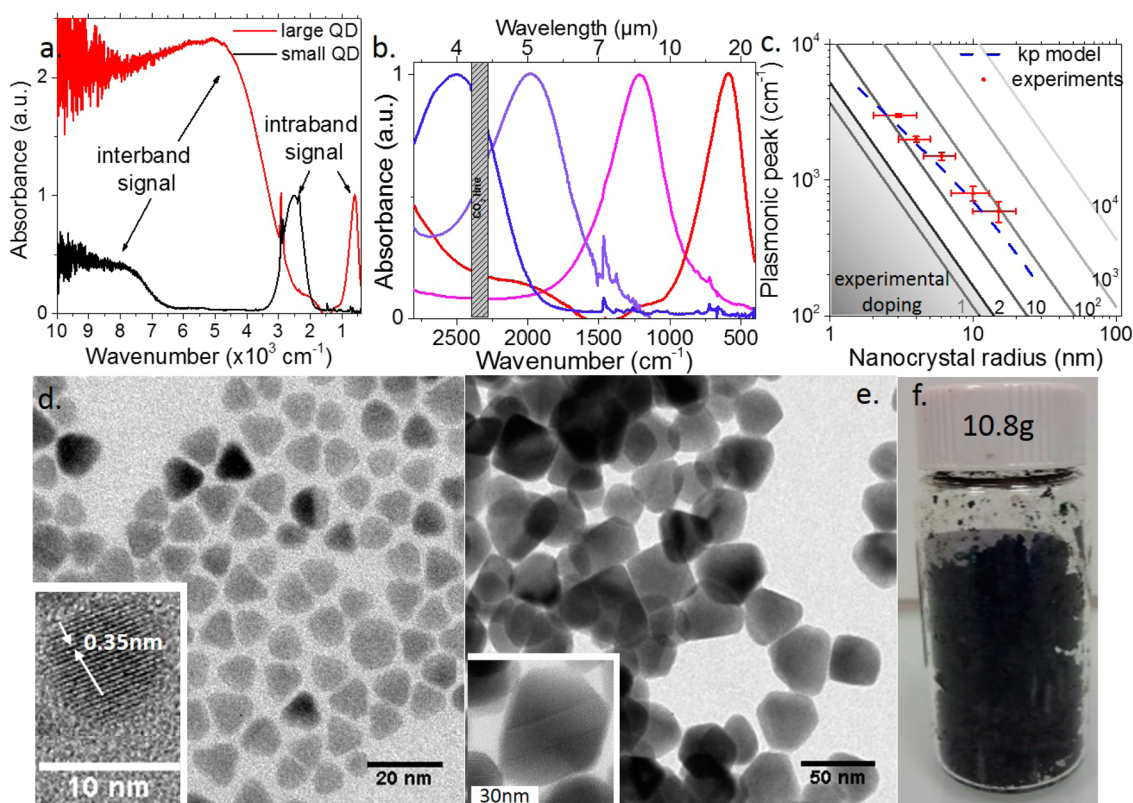


Figure 1. (a) IR absorbance for small and large HgSe CQD. (b) IR absorbance in the intraband peak range of wavenumber for HgSe CQD of different sizes. (c) Plot of the expected plasmonic peak as a function of the nanocrystal radius for different number of dopants per nanocrystal. The experimental data and their fit by a k - p model are shown in red and blue, respectively. (d) TEM image of the small HgSe CQD. The inset is a high resolution image of the nanocrystal. (e) TEM image of the large HgSe CQD. The inset is a high resolution image of the nanocrystal highlighting the polycrystalline nature of the large HgSe CQD. (f) Image of the resulting material obtained from a large scale synthesis of 10 nm HgSe CQD.

up to $300 \text{ cm}^2 \text{ V}^{-1} \text{ s}^{-1}$, which is competitive with values obtained for epitaxially grown semiconductor. Combining IR optical features with high mobility is one of the key challenges for CQD based optoelectronic. In this report we propose a method to grow CQD with optical absorption up to THz and mobilities up to $100 \text{ cm}^2 \text{ V}^{-1} \text{ s}^{-1}$. These results represent a key step toward the CQD integration into IR detectors and cameras.

To address IR optical transition one can use narrow band gap semiconductors¹³ (NBGSC) or doped semiconductors for their plasmonic properties.^{14,15} However, this second strategy does not lead to photocurrent generation and is consequently not suitable for use in photodetectors. Among NBGSC, lead chalcogenide-based CQD address the near IR,^{16,17} but cannot be pushed further because of the bulk band gap. For mid-IR,¹⁸ HgTe CQD^{19–21} have attracted most interest because of their proximity with the bulk HgCdTe alloy, extensively used for infrared detection. Recent progress has pushed the cutoff wavelength up to $12 \mu\text{m}$ using HgTe²² CQD. Unfortunately, HgTe CQD suffers from a high sensitivity to oxidation²³ due to the low electronegativity of Te, which increases the energy of the valence band. Other mercury chalcogenides present the key advantage of being self-n-doped.^{24,25} As a result, low energy absorption occurs due to intraband transition, as already commonly done in multiquantum-well heterostructure.^{26,27} So far HgSe CQD has mostly been synthesized with small sizes,²⁸ leading to excitonic features in the visible or near-IR. Aqueous phase synthesis of HgSe CQD usually lead to a poor control of the size dispersity.^{29,30} Howes et al. proposed an organic phase

synthesis³¹ for this material, but the excitonic feature remains below $1 \mu\text{m}$. Recently, improved synthesis of HgSe CQD has been proposed^{25,32} and has pushed the optical properties of HgSe CQD up to $5 \mu\text{m}$. In this report, we propose a new synthesis for HgSe CQD, which for the first time significantly expands the range of wavelength of the intraband feature up to the THz region.

We developed a synthetic method to grow HgSe CQD with tunable optical properties from 3 to $20 \mu\text{m}$. This is the reddest value reported to date for CQD and covers the mid wave and long wave atmospheric windows. The synthesis is based on the reaction of an Hg^{2+} complex with long amine and carboxylic acid chains. This precursor is fairly fragile and needs to be manipulated at low temperature ($<120 \text{ }^\circ\text{C}$). The HgSe nanocrystals present optical features in the IR made of a broad band interband transition and narrow band intraband transition, see Figure 1a–c. While introducing the Se precursor under TOPSe form, we obtained small CQD with a tunable size from 6 to 12 nm, corresponding to intraband peak transition between 3000 and 1500 cm^{-1} . The intraband absorption coefficient has been estimated to be $2300 \pm 200 \text{ cm}^{-1}$, which is consistent with a previous report.²⁵ The peak energy can be tuned by adjusting the temperature (60 to $120 \text{ }^\circ\text{C}$) and the time of the reaction (1 to 60 min). See the SI for more information about the synthetic process. The crystalline nature of the CQD appears clearly on the high resolution TEM images (see Figure 1d) and X-ray diffraction (see Figures S1 and S2). The synthesis has been scaled to greater than 10 g (Figure 1f

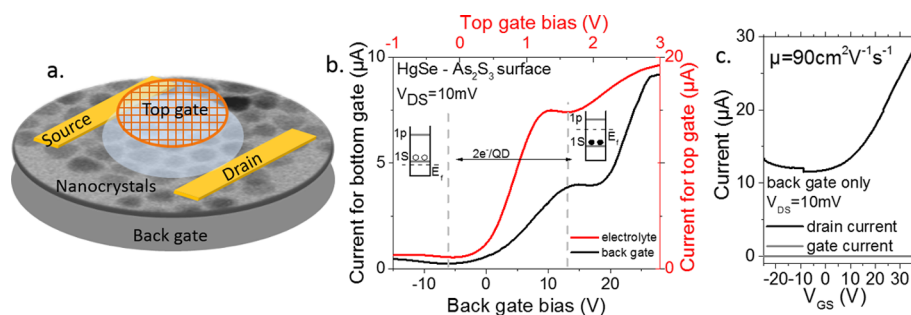


Figure 2. (a) Scheme of a dual (bottom and electrolytic) gated transistor based on a thin HgSe CQD film. (b) Transfer curve (drain current vs gate voltage) for the dual gated transistor made of a thin HgSe CQD film using back and electrolytic gating. In both cases the drain source bias is 10 mV. (c) Transfer curve for a thin HgSe CQD film using back gate only (i.e., no electrolyte is present). The film mobility is $90 \text{ cm}^2 \text{ V}^{-1} \text{ s}^{-1}$.

and S3), which is already sufficient to build a significant quantity of devices.

The trioctylphosphine acts as a ligand for these CQD and likely limits the crystal size. To grow larger CQD, we switched from Se precursor to SeS_2 , see Figure 1e. However, only the Se reacts as XRD and energy dispersive X-ray analysis revealed no sulfur content in the CQD. This result is consistent with our observation that nanoparticle formation does not take place when using TOPS instead of TopSe in the synthesis. Using SeS_2 as precursor under otherwise identical reaction conditions, the intraband feature can now be tuned within the 1500 to 500 cm^{-1} ($15 \text{ THz} \approx 60 \text{ meV}$) range, see Figure 1b (and Figures S4 to S7). The material can still absorb at $24 \mu\text{m}$ (12.5 THz), which is the limit of our spectrometer.

In the following we focus on the HgSe CQD with optical features in the $3\text{--}8 \mu\text{m}$ range and investigate their transport properties. To ensure an efficient conduction into the CQD array, we exchange the initial long and insulating ligands with As_2S_3 -based ligands. The motivation for such a choice are (i) organic ligands are not suitable due to their own absorption in the targeted range of wavelength, (ii) As_2S_3 is transparent up to $11 \mu\text{m}$, (iii) As_2S_3 has already proven its ability for high mobility film when coupled with lead³³ or mercury chalcogenides CQD.²³ Our ligand exchange procedure is inspired by the procedure of Buckley.³⁴ As_2S_3 is first dissolved in a short alkyl-chain amine.³⁵ This mixture is used to perform a phase transfer ligand exchange.⁸ As_2S_3 actually comes under a complexed form with amine,^{33,35} see Figure S8. The material is then deposited at 100°C on electrodes.

A polymer electrolyte (LiClO_4 in polyethylene glycol) is used to build a dual gated transistor, see Figure 2a. Either the back gate of the substrate (Si/SiO_2 , 400 nm of oxide) or the electrolyte gating can be used. The transfer curves are plotted on Figure 2b. The material is n-type and already doped under no gate bias as expected from the presence of intraband feature in the IR absorption. This doping is preserved even after ligand exchange (see Figure S8) since the intraband peak is still observed after the procedure. The on-off ratio is around 100. Interestingly the drain current as a function of gate bias presents two local minima, which we attribute to the complete depletion and full filling of the $1s$ state of the conduction band.³⁶

According to transport measurements, HgSe CQD contains approximately 0 to 2 electron(s) per nanocrystal. As a result the relative magnitude of the interband and intraband transition depends on the doping level. With the higher the doping, the greater the intraband absorption and the smaller the interband absorption observed. The doping is also size and surface

dependent. Such level of doping tends to confirm the intraband character of the transition instead of the plasmonic origin. First (i), because with less than 2 electrons per nanocrystal, a collective plasmonic feature is not expected to occur.³⁷ Second (ii), the plasmonic peak consistent with this density (n) of doping does not match the experimental data. Indeed, the carrier density is given by $n = \eta N_{\text{QD}} / (4/3\pi R_{\text{QD}}^3)$ with η the film density taken equal to 0.64 assuming a random close packing of the CQD, N_{QD} the number of carrier per QD, and R_{QD} the CQD radius. The plasma frequency³⁸ is then given by $\omega_p^2 = ne^2/\epsilon m$ with e the elementary charge, ϵ the dielectric constant, and m^* the carrier mass. According to the Drude model, we expect the plasmonic feature to occur at an energy

given by $\sigma_{\text{plasmon}} = \frac{1}{2\pi c} \sqrt{\frac{3\eta N_{\text{QD}} e^2}{4\pi m_e^* (\epsilon_\infty + 2\epsilon_m) R_{\text{QD}}^3}}$ where c is the speed

of light, $m_e^* = 0.05m_0 \pm 0.02$ is the effective mass in HgSe, $\epsilon_\infty = 16$ is the optical frequency dielectric constant, and $\epsilon_m = 2.1$ is the medium dielectric constant measured by ellipsometry. This plasmonic feature is expected to occur at a frequency five times lower than the observed experimental data, see Figure 1c. Moreover (iii), this intraband transition is fairly narrow compared to a usual plasmonic feature occurring in highly doped semiconductor nanocrystals.^{14,39} Finally (iv), we obtain a good agreement of the energy of the intraband transition with the computed value using a two bands $k\text{-p}$ model⁴⁰ (Figures 1c and S9); see the SI for details. With all these elements taken together, we can confidently attribute the mid- and far-infrared optical feature to an intraband transition.

The most striking transport property of this system is its extremely large carrier mobility. To obtain an accurate estimation of this mobility, we performed a measurement in a pure back gate configuration (i.e., no electrolyte), see Figure 2c.

We then extracted a mobility $\mu_n^{\text{FET}} = \frac{L}{WC_\Sigma V_{\text{DS}}} \left. \frac{\partial I_{\text{DS}}}{\partial V_{\text{GS}}} \right|_{V_{\text{DS}}}$ in the 50

to $100 \text{ cm}^2 \text{ V}^{-1} \text{ s}^{-1}$ range, which is one of the largest values reported for colloidal based material. Thanks to the high mobility of the film, the responsivity reaches 0.8 A W^{-1} (see Figure S10), meaning that the external quantum efficiency is around 20–30% for a $6 \mu\text{m}$ cutoff wavelength sample after ligand exchange. This value is typically three orders of magnitude larger than the one previously reported using HgSe CQD²⁵ and challenges the existing technology in the mid-infrared (see Figure S11). This improvement is largely attributed to the larger mobility of our sample, due to our improved ligand exchange procedure.

To further study the performance of this material for IR photodetection we have measured its electronic noise. The

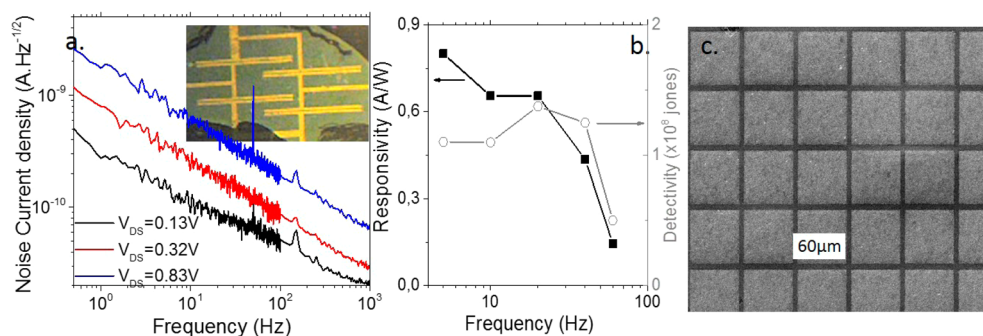


Figure 3. (a) Noise current density for a thin HgSe CQD film under three different biases. The inset is an image of the Wheatstone bridge configuration used to measure the noise. (b) Absolute photoresponse and detectivity as a function of frequency signal, under a 1 V bias at room temperature. (c) SEM picture of an array of 60 μm large pixels made in a film of HgSe CQD.

measurement is performed using a Wheatstone bridge configuration (see the inset of Figure 3a and figure S12). This approach reduces most of the DC component of the signal, which is crucial for “low” resistance sample. As expected for nanocrystals array, the noise comes under a $1/f$ form;⁴¹ see Figure 3a. The detectivity²⁶ of the device is given by $D^* = R\sqrt{A}/i_n$ with R the responsivity, A the optical area, and i_n the noise current density of the sample. Its value, at room temperature, is of the order of 10^8 jones (NEP ≈ 700 pW Hz^{-1/2}, under 1 V bias), which is similar to the one of uncooled DTGS detector. The improved mobility allows operation of the device at room temperature to achieve similar performance as at liquid nitrogen temperature of former generation of HgSe CQD based photodetectors. The 3 dB bandwidth is at 40 Hz, see Figure 3b.

Finally we investigate the use of this colloidal material as an active material of an infrared camera. In this sense it is crucial that the material can withstand the technological clean room fabrication process required for pixel design. We processed an array of pixels with sizes ranging from 20 to 60 μm (Figures 3c and S13) using e-beam lithography. The lithography step is followed by a mild plasma etching. For such sizes the pixel presents sharp edges and a high filling factor ($\sim 90\%$). The array of pixels can be as large as several millimeters and is only limited by thickness inhomogeneity of the nanocrystal film. This result is of significant interest for the design of a focal plane array based on CQD.

Conclusion. We present a new synthetic procedure for n-doped mercury chalcogenides CQDs that gives access to absorption in the mid- and far-infrared up to 25 μm . Once combined with As₂S₃ as ligand, the material can achieve mobilities as large as 100 cm² V⁻¹ s⁻¹. Compared to other CQD based devices operating at the same wavelength, our devices have a photoresponse that is three orders of magnitude larger for similar operating conditions. Alternatively it can achieve the same performances while increasing the operating temperature by 200 K. Finally we address two key steps for the integration of this material for focal plane arrays: the scale up of the colloidal synthesis (>10 g nanomaterial) and the material processing by lithography.

■ ASSOCIATED CONTENT

Supporting Information

The Supporting Information is available free of charge on the ACS Publications website at DOI: 10.1021/acs.nanolett.5b04616.

Additional data concerning the chemical preparation and material characterization of the HgSe CQD, as well as the device fabrication and optoelectronic characterization (PDF)

■ AUTHOR INFORMATION

Corresponding Authors

*E-mail: el@insp.upmc.fr.

*E-mail: benoit.dubertret@espci.fr.

Notes

The authors declare no competing financial interest.

■ ACKNOWLEDGMENTS

We thank Agence National de la Recherche for funding through grants SNAP, H2Dh, and Nanodose. This work has been supported by the Region Ile-de-France in the framework of DIM Nano-K. We thank Pr. Charles Rosenblatt and Dr. Patrick Brady for careful reading of the manuscript

■ REFERENCES

- (1) Talapin, D. V.; Lee, J. S.; Kovalenko, M.; Shevchenko, E. *Chem. Rev.* **2010**, *110*, 389–458.
- (2) Mittendorff, M.; Winnerl, S.; Kamann, J.; Eroms, J.; Weiss, D.; Schneider, H.; Helm, M. *Appl. Phys. Lett.* **2013**, *103*, 021113.
- (3) Herring, P. K.; Hsu, A. L.; Gabor, N. M.; Shin, Y. C.; Kong, J.; Palacios, T.; Jarillo-Herrero, P. *Nano Lett.* **2014**, *14*, 901–907.
- (4) Sobhani, A.; Knight, M. W.; Wang, Y.; Zheng, B.; King, N. S.; Brown, L. V.; Fang, Z.; Nordlander, P.; Halas, N. J. *Nat. Commun.* **2013**, *4*, 1643.
- (5) Koppens, F. H. L.; Mueller, T.; Avouris, Ph.; Ferrari, A. C.; Vitiello, M. S.; Polini, M. *Nat. Nanotechnol.* **2014**, *9*, 780–793.
- (6) Lhuillier, E.; Dayen, J. F.; Thomas, D. O.; Robin, A.; Doudin, B.; Dubertret, B. *Nano Lett.* **2015**, *15*, 1736.
- (7) Konstantatos, G.; Badioli, M.; Gaudreau, L.; Osmond, J.; Bernechea, M.; Pelayo Garcia de Arquer, F.; Gatti, F.; Koppens, F. H. L. *Nat. Nanotechnol.* **2012**, *7*, 363.
- (8) Nag, A.; Kovalenko, M. V.; Lee, J. S.; Liu, W.; Spokoyniy, N.; Talapin, D. V. *J. Am. Chem. Soc.* **2011**, *133*, 10612.
- (9) Koh, W. K.; Saudari, S. R.; Fafarman, A. T.; Kagan, C. R.; Murray, C. B. *Nano Lett.* **2011**, *11*, 4764.
- (10) Tang, J.; Kemp, K. W.; Hoogland, S.; Jeong, K. S.; Liu, H.; Levina, L.; Furukawa, M.; Wang, X.; Debnath, R.; Cha, D.; Chou, K. W.; Fischer, A.; Amassian, A.; Asbury, J. B.; Sargent, E. H. *Nat. Mater.* **2011**, *10*, 765.
- (11) Kovalenko, M. V.; Scheele, M.; Talapin, D. V. *Science* **2009**, *324*, 1417.
- (12) Dolzhnikov, D. S.; Zhang, H.; Jang, J.; Son, J. S.; Panthani, M. G.; Shibata, T.; Chattopadhyay, S.; Talapin, D. V. *Science* **2015**, *347*, 425.

- (13) Kershaw, S. V.; Susha, A. S.; Rogach, A. L. *Chem. Soc. Rev.* **2013**, *42*, 3033.
- (14) Luther, J. M.; Prashant, K. J.; Ewers, T.; Alivisatos, A. P. *Nat. Mater.* **2011**, *10*, 361.
- (15) Sahu, A.; Khare, A.; Deng, D.; Norris, D. J. *Chem. Commun.* **2012**, *48*, 5458.
- (16) Konstantatos, G.; Sargent, E. H. *Nat. Nanotechnol.* **2010**, *5*, 391–400.
- (17) Pietryga, J. M.; Schaller, R. D.; Werder, D.; Stewart, M. H.; Klimov, V. I.; Hollingsworth, J. A. *J. Am. Chem. Soc.* **2004**, *126*, 11752–11753.
- (18) Lhuillier, E.; Keuleyan, S.; Liu, H.; Guyot-Sionnest, P. *Chem. Mater.* **2013**, *25*, 1272–1282.
- (19) Rauch, T.; Böberl, M.; Tedde, S. F.; Fürst, J.; Kovalenko, M. V.; Hesser, G.; Lemmer, U.; Heiss, W.; Hayden, O. *Nat. Photonics* **2009**, *3*, 332.
- (20) Kovalenko, M. V.; Kaufmann, E.; Pachinger, D.; Roither, J.; Huber, M.; Stangl, J.; Hesser, G.; Schäffler, F.; Heiss, W. *J. Am. Chem. Soc.* **2006**, *128*, 3516.
- (21) Keuleyan, S.; Lhuillier, E.; Brajuskovic, V.; Guyot-Sionnest, P. *Nat. Photonics* **2011**, *5*, 489–493.
- (22) Keuleyan, S. E.; Guyot-Sionnest, P.; Delerue, C.; Allan, G. *ACS Nano* **2014**, *8*, 8676.
- (23) Lhuillier, E.; Keuleyan, S.; Zolotavin, P.; Guyot-Sionnest, P. *Adv. Mater.* **2013**, *25*, 137.
- (24) Jeong, K. S.; Deng, Z.; Keuleyan, S.; Liu, H.; Guyot-Sionnest, P. *J. Phys. Chem. Lett.* **2014**, *5*, 1139.
- (25) Deng, Z.; Jeong, K. S.; Guyot-Sionnest, P. *ACS Nano* **2014**, *8*, 11707.
- (26) Rosencher, E.; Vinter, N. *Optoelectronic*, 2nd ed; Dunod: Paris, 2002.
- (27) Lhuillier, E.; Ribet-Mohamed, I.; Nedelcu, A.; Berger, V.; Rosencher, E. *Phys. Rev. B: Condens. Matter Mater. Phys.* **2010**, *81*, 155305.
- (28) Qadri, S. B.; Kuno, M.; Feng, C. R.; Rath, B. B.; Yousuf, M. *Appl. Phys. Lett.* **2003**, *83*, 4011.
- (29) Liu, L.; Wu, Q.; Ding, Y.; Liu, H.; Zhang, B. *Colloids Surf., A* **2004**, *240*, 135.
- (30) (a) Esmaeili-Zarea, M.; Salavati-Niasaria, M.; Sobhanib, A. *Ultrason. Sonochem.* **2012**, *19*, 1079. (b) Salavati-Niasari, M.; Esmaeili-Zarea, M.; Sobhani, A. *Micro Nano Lett.* **2012**, *7*, 1300.
- (31) Howes, P.; Green, M.; Johnston, C.; Crossley, A. *J. Mater. Chem.* **2008**, *18*, 3474.
- (32) Mirzai, H.; Nordin, M. N.; Curry, R. J.; Bouillard, J.-S.; Zayats, A. V.; Green, M. *J. Mater. Chem. C* **2014**, *2*, 2107.
- (33) Yakunin, S.; Dirin, D. N.; Protesescu, L.; Sytnyk, M.; Tollabimazraehno, S.; Humer, M.; Hackl, F.; Fromherz, T.; Bodnarchuk, M. I.; Kovalenko, M. V.; Heiss, W. *ACS Nano* **2014**, *8*, 12883.
- (34) Buckley, J. J.; Greaney, M. J.; Brutchey, R. L. *Chem. Mater.* **2014**, *26*, 6311–6317.
- (35) Kovalenko, M. V.; Schaller, R. D.; Jarzab, D.; Loi, M. A.; Talapin, D. V. *J. Am. Chem. Soc.* **2012**, *134*, 2457–2460.
- (36) Yu, D.; Wang, C.; Guyot-Sionnest, P. *Science* **2003**, *300*, 1277–1280.
- (37) Pi, X.; Delerue, C. *Phys. Rev. Lett.* **2013**, *111*, 177402.
- (38) Ashcroft, N. W.; Mermin, N. D. *Solid States Physics*; CBS Publishing Asia: Hong Kong, 1987.
- (39) Rowe, D. J.; Jeong, J. S.; Mkhoyan, K. A.; Kortshagen, U. R. *Nano Lett.* **2013**, *13*, 1317.
- (40) Lhuillier, E.; Keuleyan, S.; Guyot-Sionnest, P. *Nanotechnology* **2012**, *23*, 175705.
- (41) Liu, H.; Lhuillier, E.; Guyot-Sionnest, P. *J. Appl. Phys.* **2014**, *115*, 154309.